Global Shock Buffet Instability on NASA Common Research Model

Sebastian Timme*

University of Liverpool, Liverpool, England L69 3GH, United Kingdom

A numerical study of the transonic flow over the wing of the NASA Common Research Model, specifically addressing the shock-buffet instability via global mode analysis, is discussed. Reynolds-averaged Navier–Stokes equations (coupled with a one-equation turbulence model), using an industrial computational fluid dynamics package, are used as aerodynamic model. The implicitly restarted Arnoldi iteration is applied for eigenmode computation. Large but sparse linear systems of equations, arising from shift-and-invert spectral transformation, require a sparse iterative linear equation solver. The results show how the fluid-only shock-buffet onset flow for three-dimensional wings can be linked to an absolute instability. The instability's frequency and spatial structure agree with those typically reported for similar swept-wing geometries using experimental analysis and data-based modal identification. The influence of symmetry boundary condition (for the half model) compared with the full-span configuration is scrutinised. Overall the results suggest that expensive unsteady time-marching simulations can be avoided if interest is in the incipient shock-buffet dynamics, pertinent to future edge-of-the-envelope wing design.

I. Introduction

Shock buffet on wings is an undesirable phenomenon limiting the flight envelope at high Mach numbers and load factors. Its study is critical for commercial transonic air transport. The term commonly refers to an aerodynamic instability with self-sustained shock-wave oscillations and intermittent boundary layer separation. In an industrial context, quasi-steady empirical data are usually used to decide on and design for shock-buffet onset, such as the '$\Delta\alpha = 0.1°$ offset' method and divergence of trailing edge pressure.

Shock buffet on wings comes with low amplitude shock motions and is more broadband with Strouhal numbers in the range $St = 0.2$ to 0.6 depending e.g. on sweep angle.[1] A spanwise outboard propagation of so-called *buffet cells*, which is believed to constitute the instability, has been reported both in experimental and numerical studies.[2–5] Recently, modal descriptions of shock buffet on wings has been pursued intensively. Data-based techniques, such as proper orthogonal decomposition and dynamic mode decomposition, were applied to solution snapshots of the flow over the 80%-scale Common Research Model well beyond buffet onset[6] and an older wing design close to onset conditions.[7] Identified distinct modes agree in their spatial structure and frequency content with previous observations. Using an operator-based approach instead, global mode computation on such practical cases with three inhomogeneous spatial dimensions has also been accomplished for two wing geometries.[8,9] High-Re flow investigation succeeded using the base-flow approach with the matrix operator of the Reynolds-averaged Navier–Stokes (RANS) equations plus turbulence model evaluated at a fully converged steady state. Such global mode analysis follows earlier work on aerofoil shock buffet.[10–12] While the flow unsteadiness is self-excited, not requiring structural vibration itself, resulting unsteady aerodynamic loads excite the wing structure (called buffeting) thus being detrimental to safe and comfortable flight. Taking a step towards proper aeroelastic analysis in such extreme flow conditions, forced excitation via flexible structural modes has been pursued,[13] too, identifying, besides the shock-buffet response, also a lower-frequency behaviour, which resembles previously discussed experimental data.[1,14]

With the existence of a critical global mode for wing shock buffet established,[9] we look into more detail such as using smaller increments in angle of attack and mesh refinement. The spatial structures of dominant modes are discussed for two wings, representing different generations of wing design. The paper concludes with a study of an equivalent full-span geometry with symmetry plane for the half model removed.

*Senior Lecturer, School of Engineering; sebastian.timme@liverpool.ac.uk.

II. Numerical Approach

The asymptotic time evolution of infinitesimal perturbations $\varepsilon\widetilde{\boldsymbol{u}}$ to a steady base flow $\bar{\boldsymbol{u}}$ is sought, with $\boldsymbol{u}$ containing the conservative variables of the RANS equations plus turbulence model at each grid point and $\varepsilon \ll 1$. Interest is in solutions of the form $\widetilde{\boldsymbol{u}} = \widehat{\boldsymbol{u}}e^{\lambda t}$ where $\widehat{\boldsymbol{u}}$ is the three-dimensional spatial structure of the eigenmode (i.e. right/direct eigenvector) and $\lambda = \sigma + i\omega$ describes its temporal behaviour (i.e. eigenvalue) with σ as the growth rate and ω as the angular frequency. Full linearisation of the spatial discretisation of the non-linear governing equations (including turbulence model), and substitution of the solution ansatz, leads to an algebraic system of equations,

$$J\widehat{\boldsymbol{u}} = \lambda\widehat{\boldsymbol{u}} \tag{1}$$

where the fluid Jacobian matrix J (i.e. the linearisation) is evaluated for the base flow. The implicitly restarted Arnoldi method,[15] specifically the ARPACK library,[16,17] is used to approximate a few eigenmodes of J. This approximation improves with the number of Krylov vectors and restarting is applied in practice. Hence, an effective restart of the outer iteration is essential and a polynomial approximation of that vector is used in the implementation. Convergence to wanted parts of the eigenspectrum is enhanced by applying the shift-and-invert spectral transformation with the Arnoldi iteration operating on $(J-\zeta I)^{-1}$ instead. The shift ζ defines the focus region of the search. It is thus clear that the robust and efficient solution of many linear systems of equations is desired. For this reason, the ARPACK library has been coupled with the well-exercised linear harmonic incarnation of the chosen non-linear flow solver,[18] outlined next.

The aerodynamics are simulated herein using the industry-grade DLR-TAU software package,[19,20] which solves the compressible RANS equations with a second-order, vertex-centred, finite-volume scheme. For the assumed fully turbulent flow simulations, turbulent closure via the Boussinesq eddy-viscosity assumption is achieved with the negative version of the Spalart–Allmaras model.[21] Inviscid fluxes are evaluated with a central scheme with matrix artificial dissipation, and gradients of flow variables for viscous fluxes and source terms are computed using the Green–Gauss theorem. Geometric multigrid and local time-stepping accelerate convergence to steady base-flow solutions, with the backward Euler method with lower-upper Symmetric–Gauss–Seidel iterations chosen as multigrid smoother. Unless mentioned otherwise, all steady simulations herein converged by at least 11 orders of magnitude in the density residual norm.

The linearised harmonic flow solver follows a first-discretise-then-linearise, matrix-forming philosophy with a hand-differentiated Jacobian matrix J. Linear systems arising from the shift-and-invert transformation are solved with the generalised conjugate residual algorithm with deflated restarting.[22,23] The central idea of this iterative solver, contrary to a standard restarted Krylov solver such as the generalized minimal residual algorithm[24] which discards most of the available information during restart and is hence prone to stall, is to extract the dominant vectors responsible for convergence which are found by ranking the interior eigenvalues, approximated by the Hessenberg matrix. This often results in a more robustly converging inner iteration combined with lower memory usage due to a smaller required Krylov subspace. Pivotal to an effective Krylov method is preconditioning; local block incomplete lower-upper factorisation of the shifted Jacobian matrix, blended between first- and second-order schemes, with zero level of fill-in is selected.[25]

Details of the numerical settings of the inner-outer Krylov approach, i.e. the inner sparse iterative linear equation solver and the outer iterative eigenvalue solver, are provided in table 1. All jobs ran on two and four nodes, respectively, for the half- and full-span configurations of the Common Research Model. Each node has twin Skylake 6138 processors, 40 hardware cores and 384 GB of memory.

Table 1. Numerical settings of inner-outer iterative solution strategy

Parameter	Value
Maximum number of eigenmodes per shift	$10-20$
Maximum number of outer iterations	$2-3$
Size of Krylov space for outer iterations	100
Convergence criterion on outer iterations	10^{-6}
Size of Krylov space for inner iterations	120
Number of deflation vectors for inner iterations	20
Convergence criterion on inner iterations	10^{-7}

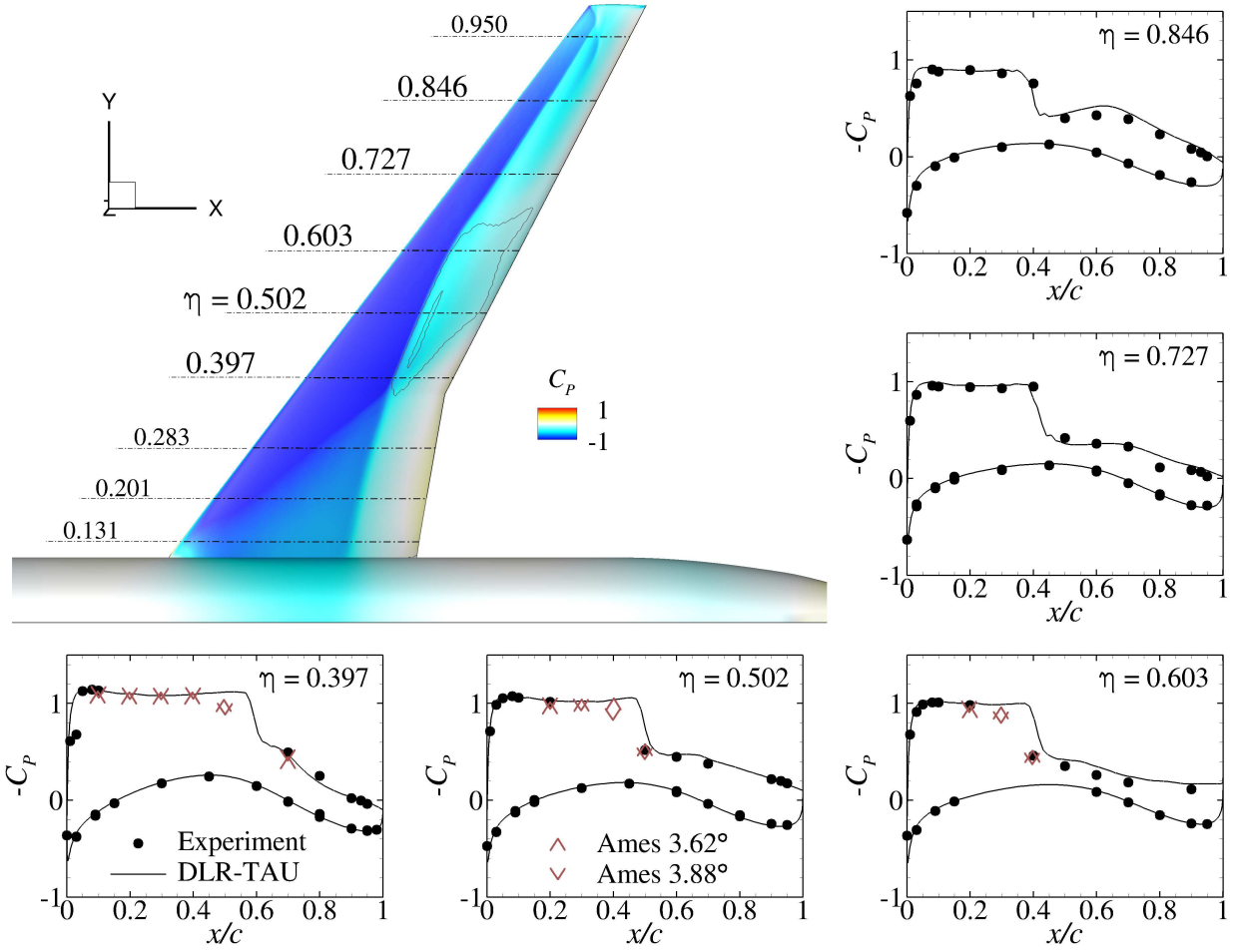

Figure 1. Surface pressure coefficient C_p at $M = 0.85$, $Re = 5$ million and $\alpha = 3.75°$ comparing experiment and steady simulation at five selected non-dimensional spanwise stations η, where flow unsteadiness is centred.

III. NASA Common Research Model

The Common Research Model is a generic wide-body aircraft configuration.[26] The wing was designed to have an aspect ratio of 9, a taper ratio of 0.275 and a 35° quarter-chord sweep angle. The mean aerodynamic chord of the wind tunnel model is 0.189 m with a span and reference area of 1.586 m and 0.280 m^2, respectively. Herein, the wing-body-tail variant with 0° tail setting angle, discarding pylon and nacelle, is analysed. The computational mesh was generated using the SOLAR mesh generator following accepted industrial practice. The experimental blade sting mounting system is excluded. The half model has about 6.2 million points including roughly 170,000 on solid wall boundaries. A viscous wall spacing of $y^+ < 1$ is ensured. The hemispherical farfield boundary is located approximately 100 semi-spans from the body, while a symmetry boundary condition is applied along the centre plane. For the full-span simulations, the half-span mesh is mirrored with respect to the xz-plane with this symmetry plane consequently removed.

Static deformation of the flexible wing at seven angles of attack was measured at certain flow conditions, specifically a Mach number of $M = 0.85$ and a Reynolds number of $Re = 5$ million per reference chord, and, to improve realism of the numerical campaign,[27] the computational mesh was deformed accordingly using a radial basis function mesh deformation tool. Figure 1 presents the wing's planform and pressure coefficient at selected spanwise stations for angle of attack of $\alpha = 3.75°$. A clear shock-wave pattern is visible along the span, and a shock-induced reverse-flow region can be observed in the mid-semi-span sector (just outboard of the Yehudi break at 37% semi-span), identified through the zero-skin-friction line. Low spatial resolution in the experimental data was addressed by incorporating related measurements of the 80%-scale Common Research Model,[4] labelled 'Ames' and showing two angles of attack bracketing the nominal value.[28]

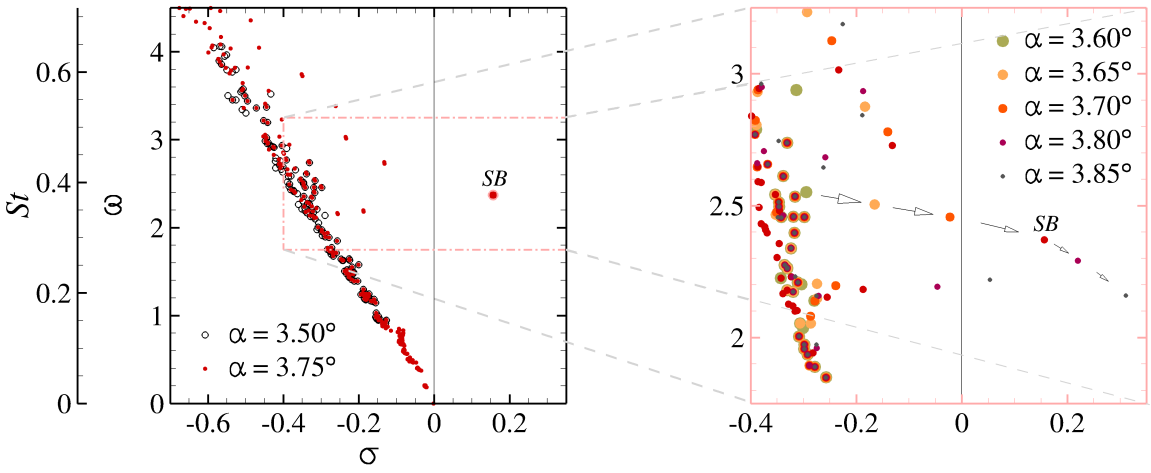

Figure 2. Computed eigenvalues for angles of attack between $\alpha = 3.50°$ and $3.85°$ showing Strouhal number St and angular frequency ω over growth rate σ. The three-dimensional shock-buffet mode with eigenvalue $(\sigma, \omega) = (0.156, 2.371)$ at $\alpha = 3.75°$ is labelled SB.

IV. Results

Details of the global stability computations with three inhomogeneous spatial dimensions, focussing on the incipient shock-buffet dynamics, are discussed in the following. The converged steady-state non-linear RANS results presented in previous section are taken as base flow. Appreciating the debate in fluid-stability theory on the treatment of the Reynolds stresses,[29,30] we follow the argument of a decoupling of scales.[11,31] Whereas the small scales of turbulence in space and time are accounted for by the turbulence model and resulting eddy viscosity, the large shock-buffet scales can be integrated in time using the unsteady RANS equations and are hence accessible for the base-flow stability approach. Previous work suggested the adequacy of unsteady RANS modelling, concerning the dominant flow features of spatial structures and frequency content, in simulating shock-buffet flow on wings, when compared to experiment and scale-resolving simulation.[5] All results are presented in non-dimensional units unless otherwise stated.

Figure 2 shows the computed eigenvalues for angles of attack where buffet onset is expected. For each angle of attack, several shifts were distributed along the imaginary axis in addition to a few shifts with positive growth rate, enabling a wider search radius albeit with a reduced convergence rate of the shift-and-invert spectral transformation. Angles of attack below (and including) $\alpha = 3.70°$ describe subcritical flow, whereas angles above (and including) $\alpha = 3.75°$ constitute a shock-buffet condition. The small increment in angle of attack of $\Delta\alpha = 0.05°$ allows the visualisation of mode traces; this is exemplified for the mode that kicks off the flow unsteadiness, labelled SB (as in shock buffet) at $\alpha = 3.75°$. The results suggest that a single unstable oscillatory global mode is responsible for shock-buffet onset on this wing similar to what was reported previously for aerofoils (see for example [10,12]). To be more precise, self-sustained oscillatory flow unsteadiness starts between angles of attack $\alpha = 3.70°$ and $3.75°$ with an angular frequency of approximately $\omega = 2.46$ (corresponding to a Strouhal number of $St = 0.39$ where $St = \omega/(2\pi)$). This value agrees nicely with the dominant frequency range reported for the 80%-scale Common Research Model in established shock-buffet condition.[6,32] While approaching the critical point, a group of eigenvalues emerges from a dense band of eigenvalues migrating towards the imaginary axis. Note that this computed dense band results from shifts placed along the imaginary axis and the convergence properties of shift-and-invert methods, and a dense cloud of eigenvalues to the left of the visible band (similar to spectra for small aerofoil cases) is expected. Specifically, besides the primary rightmost eigenvalue denoted SB, eigenvalues with increased growth rate can be observed for Strouhal numbers $St \approx 0.3$ to 0.7, which is consistent with the accepted broadband-frequency range reported for wings[1] and hints at additional unstable modes for post-onset angles of attack. Indeed, a second instability is observed at $\alpha = 3.85°$ in the same frequency range.

The spatial structure of the unstable global mode SB at $\alpha = 3.75°$ is presented in figure 3, visualising buffet cells. The term *buffet cell* refers to a local flow arrangement of a ripple along the spanwise shock-wave combined with a pulsating recirculation bubble, which develops within a restricted sector of the wingspan. Spatial amplitudes of the shock-buffet mode are concentrated at the shock wave (weakly, presumably due

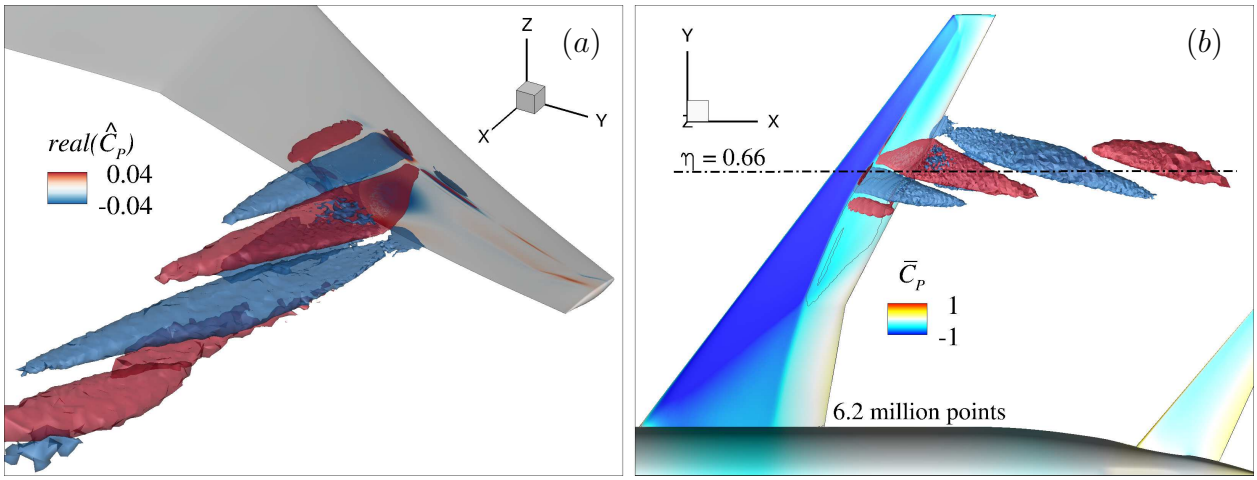

Figure 3. Spatial structure of unstable eigenmode SB showing volumetric iso-surfaces for two values ($\pm$0.02) of x-momentum component $\widehat{\rho u}$ and in (a) real part of surface pressure coefficient $\widehat{C}_p$ calculated from eigenvector and (b) surface pressure coefficient $\bar{C}_p$ and zero-skin-friction line of base flow. Eigenvector has been scaled by the maximum value in x-momentum, found at approximately $(x, y, z) = (1.170, 0.546, 0.160)$.

to mesh coarseness) and its downstream shear layer. In the figure only the real part of the complex-valued eigenvector, scaled by the maximum value in x-momentum component, is shown since the imaginary part is 90° out-of-phase to enable the convection of flow structures.[10,31] The propagation path of these buffet-cell structures is chordwise downstream and spanwise outboard, while there is wing support in the sector $\eta \approx 0.6$ to 0.73, and then downstream in the wake, reaching beyond the x-location of the horizontal-tail plane. It is interesting to observe that the spatial structures of the three-dimensional shock-buffet mode originate at the wing surface near the outermost portion of the reverse flow region, as enclosed by the base-flow zero-skin-friction line in figure 3(b) just outboard of the Yehudi break. Since the sign of the skin-friction coefficient is based on the x-velocity component, this suggests that the buffet cells emerge in the vicinity of where reversed flow is forced to turn back into the main streamwise flow direction. Inspection of the other eigenmodes with increased growth rate (cf. figure 2 for Strouhal numbers $St \approx 0.3$ to 0.7) is presented in figure 5 below.

In figure 4 (together with figure 3(b) for the top view on the medium mesh) a mesh-convergence study is offered to build confidence in the shock-buffet physics presented herein. A coarser (3.1 million points) and a finer (8.2 million points) mesh of the same family are investigated. The slices in the right column, showing the real part of x-momentum component $\widehat{\rho u}$, are taken at constant $\eta = 0.660$, which locates them approximately at the centre of the three-dimensional spatial structure. Gradually converging results with respect to the mesh density are confirmed; for instance, the features of the spatial structure become more refined with decreasing mesh spacing. Concerning the corresponding eigenvalues (cf. table 2), it is the rightmost eigenvalue in the shock-buffet frequency range, identified in either case. Whereas the growth rate on the coarsest mesh with 3.1 million points still indicates stable conditions, the two finer meshes predict the instability. Despite a remaining sensitivity in growth rate, the frequencies agree nicely throughout.

Figure 5 shows a portion of the eigenspectrum, where the pure-aerodynamic shock-buffet instability is found, at three angles of attack around onset together with the spatial structure of a number of physically dominant eigenvectors at $\alpha = 3.75°$. A correlation between the modes' frequencies and their spatial

Table 2. Mesh convergence of rightmost shock-buffet eigenmode

Mesh points (in million)	Eigenvalue (σ, ω)
3.1	$-0.163, 2.330$
6.2	$0.156, 2.371$
8.4	$0.115, 2.361$

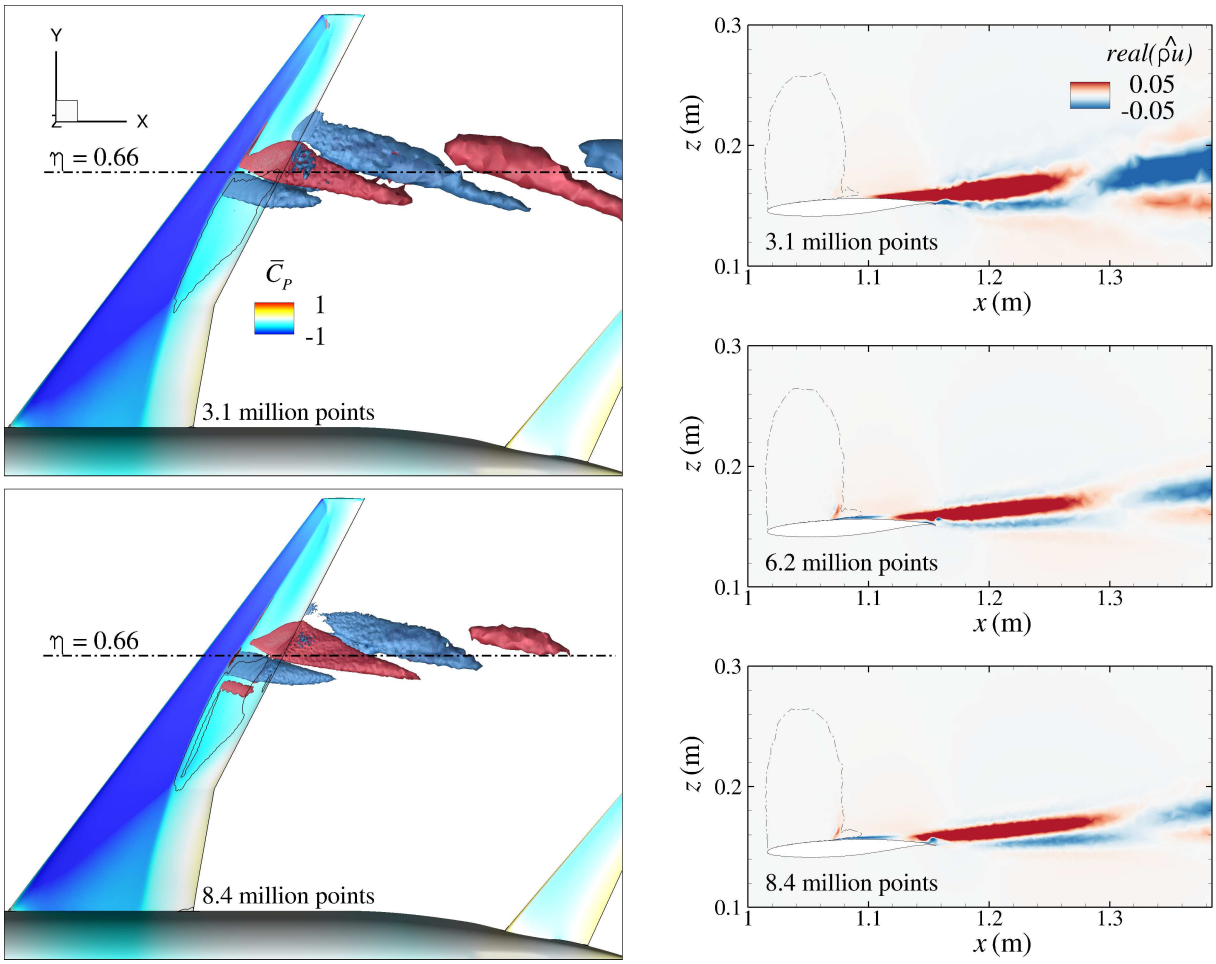

Figure 4. Mesh refinement for spatial structure of rightmost eigenmode showing (left column) volumetric iso-surfaces for two values ($\pm$0.02) of the x-momentum component $\widehat{\rho u}$ for coarsest and finest mesh (see figure 3(b) for medium mesh) and (right column) real part of x-momentum at constant spanwise station $\eta = 0.660$. The sonic line is highlighted by a dash-dotted line. Eigenvectors have been scaled by their respective maximum value in x-momentum for the purpose of comparing results on different meshes.

structures, represented by volumetric iso-surfaces of the real part of x-momentum $\widehat{\rho u}$ at non-dimensional values of ± 0.02, is evident. Eigenvectors have been normalised by their respective x-momentum value at $(x, y, z) = (1.170, 0.546, 0.160)$, which is the location of the maximum value for mode b in the figure (which is mode SB; cf. figure 3(b)), to set the phase at this point consistently to zero throughout. The richness in frequencies and spatial structures could explain the often-reported broadband-frequency nature of shock buffet on wings, which is in contrast to aerofoil studies.[10,12] Besides the five modes with their spatial structures shown, there is a large number of modes in this same frequency range, which do not emerge from the dense band/cloud of eigenvalues but do have a strong contribution from similar coherent structures; yet, those modes also feature increasingly incoherent contributions between the near- and far-field domain.

For the sake of supporting the statements made herein, stability results, analogous to figure 5, are also presented for an older (1970s) wing design for which extensive unsteady experimental data from advanced optical techniques are available[3,7,14] and various numerical studies have addressed this experiment, too.[5,7,8] The test case, referred to as RBC12, is a half wing-body configuration scaled to wind tunnel dimensions with a quarter-chord sweep angle of 25°, a reference area of 0.296 m^2, an aerodynamic mean chord of 0.279 m, a semi-span of 1.104 m and an aspect ratio of 7.78. Results are presented for the design Mach number of 0.80 and Reynolds number (based on the aerodynamic mean chord) of 3.75 million. Figure 6 shows the same portion of the eigenspectrum (cf. figure 5), where the pure-aerodynamic shock-buffet instability is suspected. Specifically, these results have previously been published in [8] and herein we complement those eigenvalues

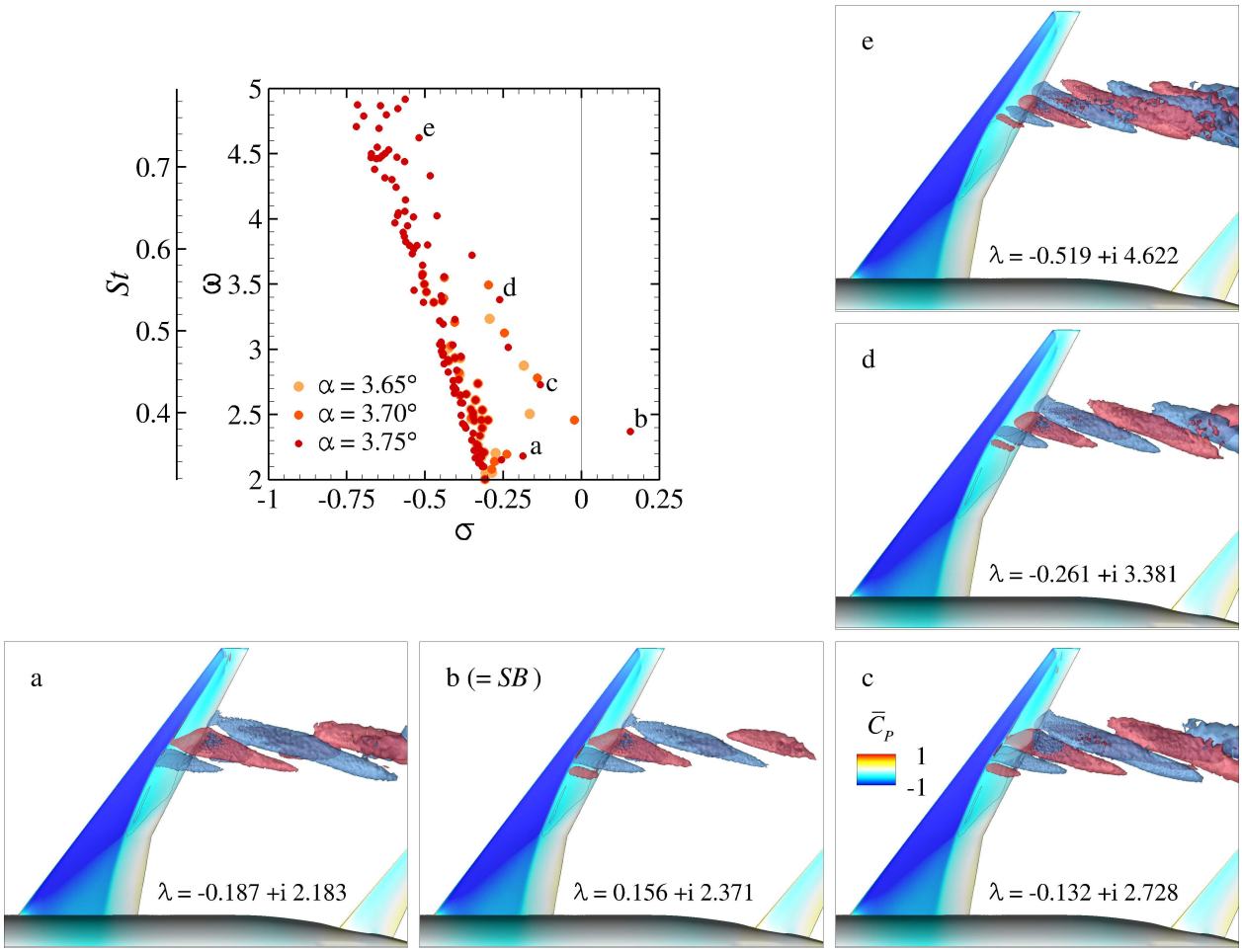

Figure 5. Stability results for Common Research Model wing at $M = 0.85$ and $Re = 5$ million showing both eigenvalue spectra at three angles of attack approaching (and beyond) shock-buffet onset and corresponding spatial structure of representative modes at $\alpha = 3.75°$ as two iso-surfaces of real part of x-momentum component $\widehat{\rho u}$ at non-dimensional values of ± 0.02. Eigenvectors have been normalised by the x-momentum value at $(x, y, z) = (1.170, 0.546, 0.160)$ to set the phase at this point consistently to zero throughout. Wing-surface colouring describes steady pressure coefficient $\bar{C}_p$, while solid line is zero skin-friction line.

by corresponding spatial structures. Eigenvalue results at three sub-critical angles of attack are presented. The clear migration of dominant eigenvalues due to the small increment in angle of attack of a hundredth degree highlights that the absolute instability is imminent. Note that shock-buffet onset is expected at angle of attack $\alpha \approx 3.05°$ based on time-marching unsteady RANS simulations.[8] Even though the absolute instability is rightly not computed in the considered angle-of-attack range, due to non-converging steady-state simulations to obtain the base flow in the vicinity of onset and the currently available matrix-forming non-time-stepping stability tools, a significant change in the spatial structure of the dominant oscillatory modes is not expected and hence these give a good indication of the disturbance physics. A similar observation compared with the Common Research Model wing can be made; coherent structures related to the shock-buffet instability are centred near the outermost stations of the reverse-flow region in the steady flow field, albeit it being shifted closer towards the wing tip. Also, a large number of additional modes in this range exhibit increasingly incoherent features next to having a strong contribution from the described coherent shock-buffet structures. Frequencies and growth rates of the physically relevant (i.e. non-spurious) modes approaching the imaginary axis are similar near shock-buffet onset for the two wing designs.

Those additional eigenmodes could play a role in explaining the often-reported (and widely-accepted) broadband-frequency nature of wing shock buffet beyond onset conditions. Recall that the analysis herein targets the onset of the alleged Hopf oscillator, called shock buffet, and not established shock-buffet conditions. A second contributing point in this discussion concerns the inherent non-linearity of the dynamics

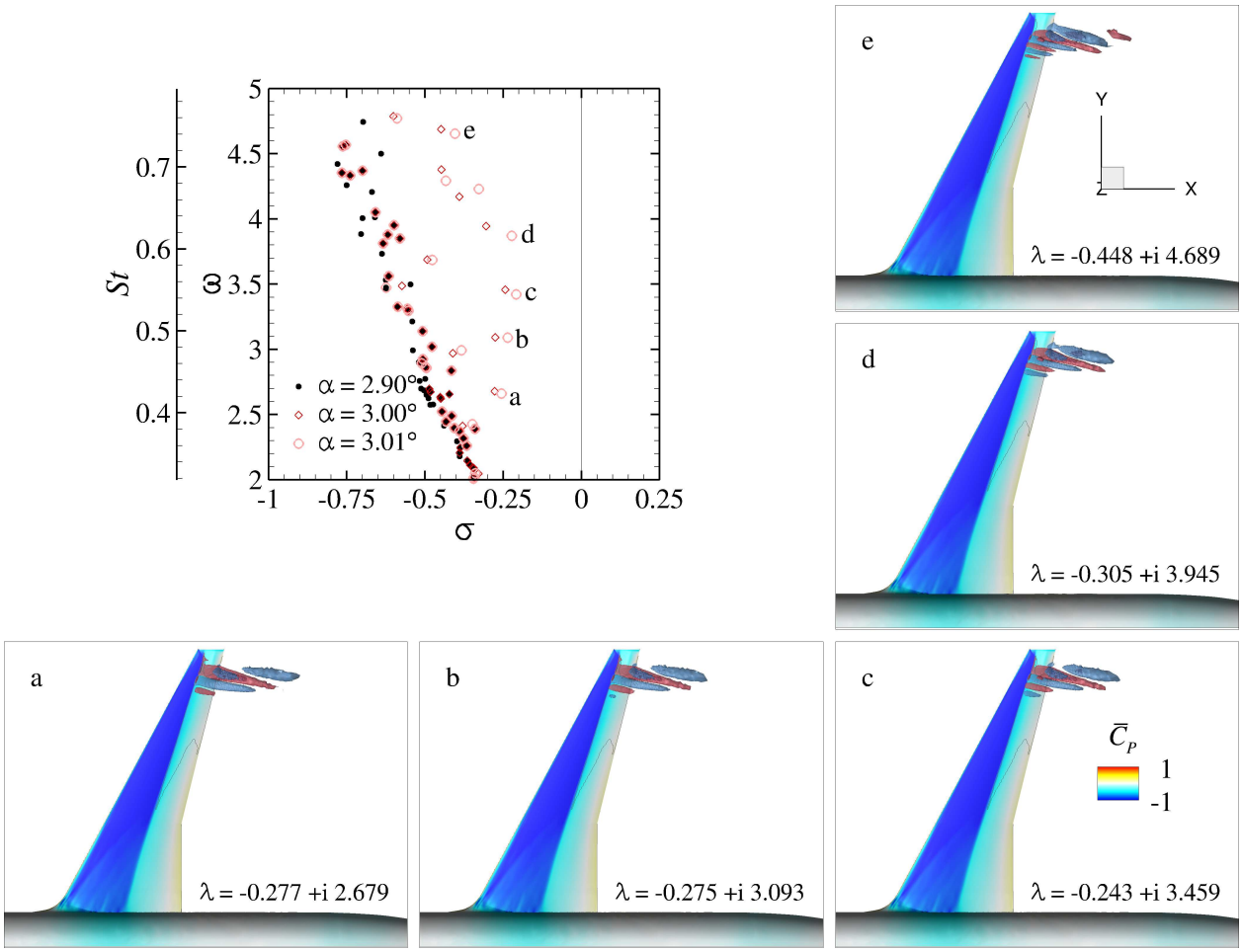

Figure 6. Stability results for RBC12 wing at $M = 0.80$ and $Re = 3.75$ million showing both eigenvalue spectra at three angles of attack below shock-buffet onset and corresponding spatial structure of representative modes at $\alpha = 3.00°$ as two iso-surfaces of real part of x-momentum component $\widehat{\rho u}$ at non-dimensional values of ± 0.02. Eigenvectors have been normalised by the x-momentum value at $(x, y, z) = (0.546, 1.010, 0.063)$ to set the phase at this point consistently to zero throughout. Wing-surface colouring describes steady pressure coefficient $\bar{C}_p$, while solid line is zero skin-friction line.

of shock-wave/boundary-layer interaction, which is elucidated below with the help of figure 7(b). Thirdly, when thoroughly comparing with experimental data, the flexible wing structure must not be ignored at these high wing-loading conditions, which makes the fluid-only shock-buffet instability and the structural buffeting response a multidisciplinary challenge indeed. The current RANS results shed light on a pure aerodynamic instability but at the same time cannot explain everything that is going on in the wind tunnel. For instance, [14] reported distinct lower-frequency shock dynamics, with an inboard propagation direction and widely extending along the span. The frequency content is stated to be in the range of aerofoil shock-buffet frequencies, whether this is coincidental or not. Similar behaviour was mentioned in [1]. Numerically, small-amplitude forced wing vibration also showed resonant aerodynamic response for $St \approx 0.1$, besides the accepted shock-buffet range with $St \approx 0.3$ to 0.7.[8,13] In any case, our computations paid special attention to this lower-frequency range trying to identify another absolute instability mechanism, without success. Nevertheless, these findings for transonic flow over wings do not rule out an instability of convective nature (i.e. a noise amplifier) and pseudo-resonance due to the non-normality of the governing equations.[12,31,33]

It is intriguing to also note a recent biglobal stability analysis in [34] on infinite-span geometries assessing wing-sweep effects. *Biglobal* refers to a stability analysis in three-dimensional space with two inhomogeneous dimensions.[35] The third (homogeneous) direction is treated as periodic with spanwise wavenumber β. The authors contemplate unstable spatial (monotone) modes adding a spanwise three-dimensional structure to a nominally aerofoil shock-buffet mode for the unswept wing, which turn into propagating oscillatory modes

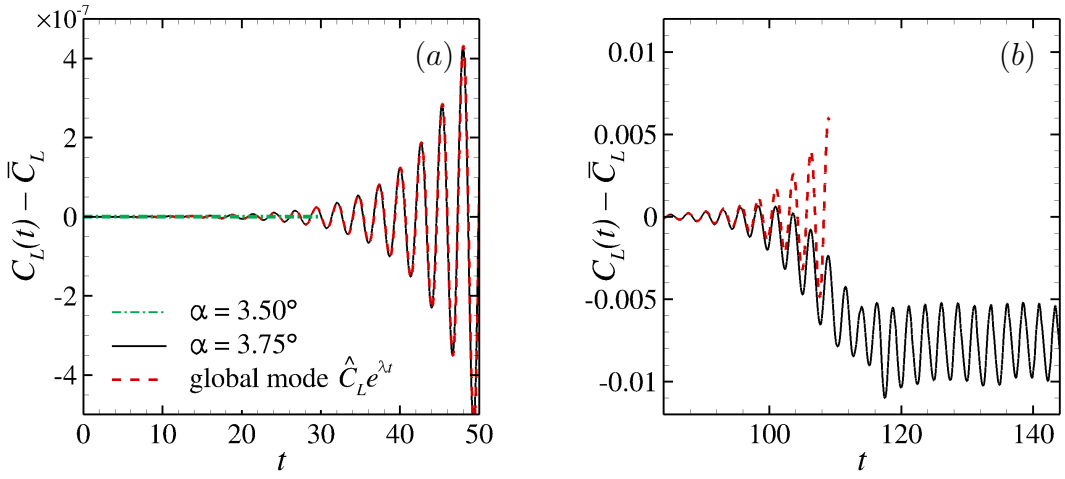

Figure 7. Time histories of lift coefficient around base-flow solution, $C_L(t) - \bar{C}_L$, showing (*a*) initial linear regime from time-marching unsteady RANS simulations, bracketing onset between $\alpha = 3.50°$ and $3.75°$, and comparison with signal reconstructed from unstable mode at $\alpha = 3.75°$ and (*b*) effect of non-linear saturation.

when wing sweep is imposed. The authors link their co-existing lower- and higher-frequency modes to the work reported in [1], and that discussion should be expanded in view of results in [7,8,13,14]. Notwithstanding the *triglobal* stability analysis on a finite-span (i.e. without periodic boundaries) and swept wing conducted herein, which cautions juxtaposition, the consensus in salient shock-buffet features is interesting indeed.

To further support the findings, time-marching unsteady RANS results are presented in figure 7. The governing equations are integrated in time using dual-time stepping, while monitoring convergence with a Cauchy criterion on the drag coefficient with a relative error tolerance of 10^{-8}. Criteria on iterations and the chosen time-step size ($\Delta t = 1\,\mu s$) follow previous studies.[5] The figure shows the perturbation of lift coefficient around the base-flow solution, $C_L(t) - \bar{C}_L$, as a function of non-dimensional time t. Specifically, conventional time-marching results at $\alpha = 3.75°$ are compared with the unsteady lift coefficient calculated from the unstable global mode using the relation $\widetilde{C}_L(t) = \widehat{C}_L\, e^{\lambda t} + \text{c.c.}$, where c.c. refers to complex conjugate. The latter equation ensures that a real-valued physical signal is reconstructed from the complex-valued eigenmode, with the eigenvector prescribing the magnitude and phase at the mesh points and oscillation frequency and exponential envelope function provided by the eigenvalue. Conveniently, the amplitude of the unsteady lift coefficient, denoted $\widehat{C}_L$, is calculated directly from the eigenvector using the expression $\widehat{C}_L = \partial C_L / \partial \boldsymbol{u} \cdot \widehat{\boldsymbol{u}}$, which is widely known in the context of (dynamic) derivative and adjoint gradient computations. The partial derivative with respect to the state variables, computed once and for all for the base flow, generalises to any integrated aerodynamic load of interest. This makes post-processing very effective without the need otherwise to feed the computed unsteady field solution of the conservative variables, which can also be reconstructed from the base flow and eigenmode, back into the non-linear flow solver. Since the linear eigenvector $\widehat{\boldsymbol{u}}$ can be scaled arbitrarily, and the time-marched solution is integrated in time from an initial condition of white noise, its magnitude is adjusted manually to align with the time-domain results.

In figure 7(*a*), time histories of the lift coefficient locate the onset of shock-buffet instability between $\alpha = 3.50°$ and $3.75°$. No attempt is made to refine this bracket further using time-marching simulations. Agreement between the conventional time-marching simulation and global stability analysis is excellent in the linear-amplitude range. Since the underlying physics of wing shock buffet is highly non-linear, non-linear saturation leading to limit-cycle oscillation is expected. This behaviour is presented in figure 7(*b*). With a base-flow lift coefficient of $\bar{C}_L = 0.606$, the amplitude non-linearity takes over when the unsteady perturbation in lift coefficient reaches about 0.1% of its base-flow value. The terminal limit-cycle amplitude reaches about 0.4% of the base-flow value with its time-averaged mean dropping about 1.2% below the base-flow lift coefficient. The low limit-cycle amplitude confirms the vicinity to the instability onset for angle of attack $\alpha = 3.75°$. Also observe the rather regular oscillations in the non-linear regime. Recall that stability analysis of the steady base flow, which is a solution of the discretised non-linear three-dimensional RANS equations (plus turbulence model), is performed herein. In contrast, the time-averaged mean flow is not such an equilibrium solution. Subtleties of this distinction have been discussed in the past.[31,36]

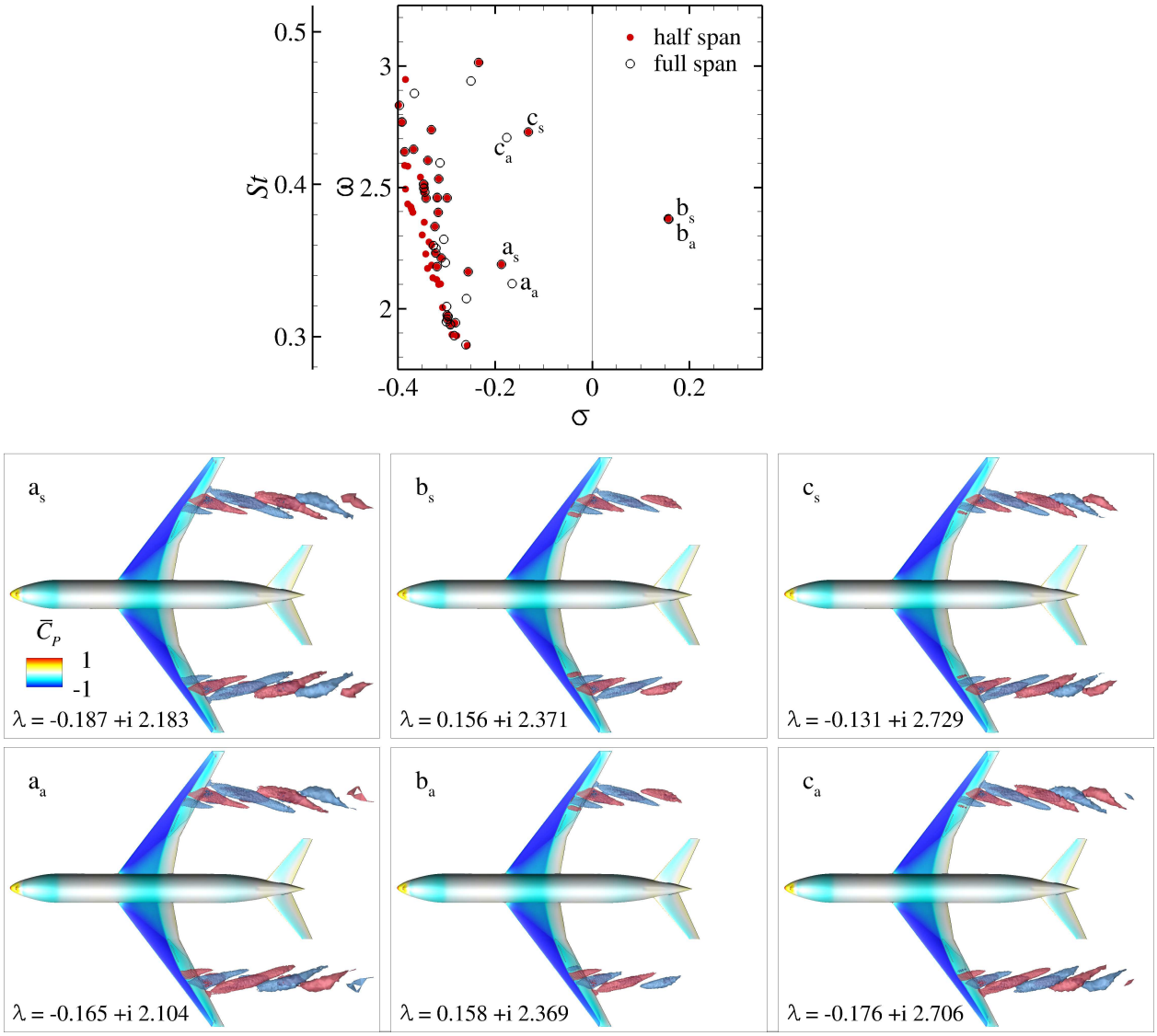

Figure 8. Stability results for Common Research Model wing at $M = 0.85$, $Re = 5$ million and $\alpha = 3.75°$ showing both eigenvalue spectra for half- and full-span computations and corresponding spatial structure of representative full-span modes as two iso-surfaces of real part of x-momentum component $\widehat{\rho u}$ at non-dimensional values of ± 0.02. Eigenvectors have been scaled by the x-momentum at $(x, y, z) = (1.170, 0.546, 0.160)$ to set the phase at this point consistently to zero throughout. Wing-surface colouring describes steady pressure coefficient $\bar{C}_p$, while solid line is zero skin-friction line. Subscripts s and a indicate symmetric and anti-symmetric modes, respectively. Symmetric modes correspond to half-model results in figure 5 (modes a, b and c).

The presentation of results concludes with the preliminary study of the impact of (not) enforcing a symmetry boundary condition at the fuselage centre plane for the Common Research Model configuration. Figure 8 shows the relevant part of the eigenspectra for the half- and full-span models at angle of attack $\alpha = 3.75°$. Labelling of eigenmodes follows figure 5. We observe pairs of eigenvalues (not referring to the complex conjugate pairs), labelled with subscripts s and a for symmetric and anti-symmetric, respectively. The unstable eigenvalue seems to have approximately algebraic multiplicity of 2 (appreciating that we use iterative solution schemes with approximate linear solves). For the remaining dominant eigenvalues, one of each pair coincides with the half-span result, while the second is slightly shifted. Note that these pairs were calculated independent of the chosen shift ζ. Importantly, the corresponding pairs of eigenvectors show symmetric and anti-symmetric behaviour. Specifically, for the symmetric case, all conservative variables are mirrored with respect to the fuselage centre plane, e.g. $\widehat{\rho u}_{\text{left}} = \widehat{\rho u}_{\text{right}}$, except the y-momentum component

with $\widehat{\rho v}_{\text{left}} = -\widehat{\rho v}_{\text{right}}$, and vice versa for the anti-symmetric modes. The symmetric full-span modes agree with the half-span results, as expected, since symmetry boundary condition is enforced in the half-span simulation. The occurrence of anti-symmetric modes means that the dynamic manifestation of the shock-buffet instability on port and starboard sides of the aircraft does not have to be synchronised.

V. Conclusions

Eigenmodes of a practical test case with three inhomogeneous spatial dimensions, specifically an aircraft wing in high-Re turbulent and transonic flow, have been computed. A matrix-forming iterative scheme of an inner-outer Krylov structure, implemented in an industrial Reynolds-averaged Navier–Stokes flow solver, succeeds in identifying an absolute instability linked to shock-buffet onset on a wing for the first time. These fundamental results suggest that the incipient departure of shock-buffet unsteadiness from a non-linear steady base flow is governed by the dynamics of a single unstable oscillatory eigenmode, which eventually is superseded by effects of non-linear saturation. Increasing the angle of attack beyond onset condition, additional modes from a group of modes, exhibiting increased growth rates in the vicinity of instability onset and lying within the broadband-frequency range typical reported for transport-type wings, become unstable. Specifically for the wing of the NASA Common Research Model discussed herein, the investigated flow condition is a Mach number of 0.85 with reference-chord Reynolds number of 5 million. Onset occurs just above the angle of attack of 3.70° with a Strouhal number of approximately 0.39. The spatial structure of the unstable mode itself confirms what has been coined shock-buffet cells and inferred previously from numerical and experimental studies on wings. Addressing the symmetric and anti-symmetric characteristics, which is routinely done in more fundamental fluid-stability studies, the full-span configuration shows that pairs (not referring to the complex conjugate pairs, which exist, too) of eigenmodes emerge describing complementary symmetric and anti-symmetric spatial structures.

The numerical findings are surprising in light of the often-used broadband-frequency explanation of three-dimensional shock buffet and have far-reaching implications, going beyond a mere better understanding of edge-of-the-envelope flow physics. This study will inform routes to buffet control via eigenvalue sensitivity and when attempting to establish rapid shock-buffet prediction tools for routine industrial unsteady aerodynamic analysis, such as reduced order models based on a modal-decomposition-and-projection philosophy. The adapted industrial flow solver paves the way to exploit concepts, established in fundamental fluid mechanics on mostly canonical test cases, in an applied and practical setting. It is anticipated that higher-fidelity eddy-resolving simulations, to overcome well-known inherent issues of turbulence modelling, will reveal the same low-frequency buffet modes albeit a variety of associated feature-rich phenomena. With an absolute instability confirmed, the role of convective mechanisms in shock-buffet flow physics on wings remains to be scrutinised. In the long-term, fully-coupled fluid-structure analysis is desirable when considering the innate multidisciplinary nature of such edge-of-the-envelope flight physics.

Acknowledgements

The author is grateful to colleagues at Aircraft Research Association Ltd. (A. Peace) for providing the meshes and German Aerospace Center (S. Keye) for discussing the wind tunnel data.

References

[1]Dandois, J., "Experimental study of transonic buffet phenomenon on a 3D swept wing," *Phys. Fluids*, Vol. 28, 2016.

[2]Iovnovich, M. and Raveh, D. E., "Numerical Study of Shock Buffet on Three-Dimensional Wings," *AIAA J.*, Vol. 53, No. 2, 2015, pp. 449–463.

[3]Lawson, S., Greenwell, D., and Quinn, M. K., "Characterisation of Buffet on a Civil Aircraft Wing," *54th AIAA Aerospace Sciences Meeting, AIAA SciTech Forum*, 2016, AIAA 2016-1309.

[4]Koike, S., Ueno, M., Nakakita, K., and Hashimoto, A., "Unsteady Pressure Measurement of Transonic Buffet on NASA Common Research Model," *34th AIAA Applied Aerodynamics Conference, AIAA AVIATION Forum*, 2016, AIAA 2016-4044.

[5]Sartor, F. and Timme, S., "Delayed Detached-Eddy Simulation of Shock Buffet on Half WingBody Configuration," *AIAA J.*, Vol. 55, No. 4, 2017, pp. 1230–1240.

[6]Ohmichi, Y., Ishida, T., and Hashimoto, A., "Modal Decomposition Analysis of Three-Dimensional Transonic Buffet Phenomenon on a Swept Wing," *AIAA J.*, Vol. Articles in Advance, 2018.

[7]Masini, L., Timme, S., and Peace, A. J., "Scale-resolving simulation of shock buffet onset physics on a civil aircraft wing," *Royal Aeronautical Society 2018 Applied Aerodynamics Conference*, 2018.

[8]Timme, S. and Thormann, R., "Towards three-dimensional global stability analysis of transonic shock buffet," *AIAA AVIATION Forum*, 2016, AIAA 2016-3848.

[9]Timme, S., "Global instability of wing shock buffet," *arXiv e-prints*, 2018, arXiv:1806.07299 [physics.flu-dyn].

[10]Crouch, J. D., Garbaruk, A., and Magidov, D., "Predicting the onset of flow unsteadiness based on global instability," *J. Comput. Phys.*, Vol. 224, No. 2, 2007, pp. 924–940.

[11]Crouch, J. D., Garbaruk, A., Magidov, D., and Travin, A., "Origin of transonic buffet on aerofoils," *J. Fluid Mech.*, Vol. 628, 2009.

[12]Sartor, F., Mettot, C., and Sipp, D., "Stability, receptivity and sensitivity analyses of buffeting transonic flow over a profile," *AIAA J.*, Vol. 53, No. 7, 2015, pp. 1980–1993.

[13]Belesiotis-Kataras, P. and Timme, S., "Numerical Study of Incipient Transonic Shock Buffet on Large Civil Aircraft Wings," *Royal Aeronautical Society 2018 Applied Aerodynamics Conference*, 2018.

[14]Masini, L., Timme, S., Ciarella, A., and Peace, A., "Influence of vane vortex generators on transonic wing buffet: further analysis of the BUCOLIC experimental dataset," *Proceedings of the 52nd 3AF Intern. Conf. on Applied Aerodynamics, Lyon, France (2017)*, 2017.

[15]Sorensen, D. C., "Implicit Application of Polynomial Filters in a k-Step Arnoldi Method," *SIAM J. Matrix Anal. Appl.*, Vol. 13, No. 1, 1992, pp. 357–385.

[16]Lehoucq, R., Sorensen, D., and Yang, C., *ARPACK Users' Guide*, SIAM, 1998.

[17]Maschhoff, K. J. and Sorensen, D. C., "P_ARPACK: An efficient portable large scale eigenvalue package for distributed memory parallel architectures," *Lecture Notes in Computer Science*, Vol. 1184, 1996, pp. 478–486.

[18]Thormann, R. and Widhalm, M., "Linear-frequency-domain predictions of dynamic-response data for viscous transonic flows," *AIAA J.*, Vol. 51, No. 11, 2013, pp. 2540–2557.

[19]Schwamborn, D., Gerhold, T., and Heinrich, R., "The DLR TAU-Code: recent applications in research and industry," *European Conference on Computational Fluid Dynamics*, 2006, ECCOMAS CFD 2006.

[20]Langer, S., "Agglomeration multigrid methods with implicit Runge–Kutta smoothers applied to aerodynamic simulations on unstructured grids," *J. Comput. Phys.*, Vol. 277, 2014, pp. 72–100.

[21]Allmaras, S. R., Johnson, F. T., and Spalart, P. R., "Modifications and Clarifications for the Implementation of the Spalart–Allmaras Turbulence Model," *ICCFD7-1902, 7th Intern. Conf. on Computational Fluid Dynamics, Big Island, Hawaii, 9-13 July 2012*, 2012.

[22]Parks, M. L., de Sturler, E., Mackey, G., Johnson, D. D., and Maiti, S., "Recycling Krylov subspaces for sequences of linear systems," *SIAM J. Sci. Comput.*, Vol. 28, No. 5, 2006, pp. 1651–1674.

[23]Xu, S., Timme, S., and Badcock, K. J., "Enabling off-design linearised aerodynamics analysis using Krylov subspace recycling technique," *Computers and Fluids*, Vol. 140, 2016, pp. 385–396.

[24]Saad, Y. and Schultz, M. H., "GMRES: A Generalized Minimal Residual Algorithm for Solving Nonsymmetric Linear Systems," *SIAM J. Sci. Stat. Comput.*, Vol. 7, No. 3, 1986, pp. 856–869.

[25]McCracken, A., Da Ronch, A., Timme, S., and Badcock, K. J., "Solution of linear systems in Fourier-based methods for aircraft applications," *Int. J. Comput. Fluid Dyn.*, Vol. 27, No. 2, 2013, pp. 79–87.

[26]Vassberg, J. C., DeHaan, M. A., Rivers, S. M., and Wahls, R. A., "Development of a common research model for applied CFD validation studies," *26th AIAA Applied Aerodynamics Conference*, 2008, AIAA 2008-6919.

[27]Tinoco, E. N., Brodersen, O., Keye, S., and Laflin, K., "Summary of data from the Sixth AIAA CFD drag prediction workshop: CRM Cases 2 to 5," *55th AIAA Aerospace Sciences Meeting, AIAA SciTech Forum*, 2017, AIAA 2017-1208.

[28]Tinoco, E. N., Brodersen, O., Keye, S., Laflin, K., Feltrop, E., Vassberg, J. C., Mani, M., Rider, B., Wahls, R. A., Morrison, J. H., Hue, D., Roy, C. J., Mavriplis, D. J., and Murayama, M., "Summary Data from the Sixth AIAA CFD Drag Prediction Workshop: CRM Cases," *J. Aircraft*, Vol. 55, No. 4, 2018, pp. 1352–1379.

[29]Reynolds, W. C. and Hussain, A. K. M. F., "The mechanics of an organized wave in turbulent shear flow. Part 3. Theoretical models and comparisons with experiments," *Journal of Fluid Mechanics*, Vol. 54, No. 2, 1972, pp. 263–288.

[30]Mettot, C., Sipp, D., and Bézard, H., "Quasi-laminar stability and sensitivity analyses for turbulent flows: Prediction of low-frequency unsteadiness and passive control," *Phys. Fluids*, Vol. 26, 2014, pp. 045112.

[31]Sipp, D., Marquet, O., Meliga, P., and Barbagallo, A., "Dynamics and Control of Global Instabilities in Open-Flows: A Linearized Approach," *ASME. Appl. Mech. Rev.*, Vol. 63, No. 3, 2010, pp. 030801.

[32]Sugioka, Y., Koike, S., Nakakita, K., Numata, D., Nonomura, T., and Asai, K., "Experimental analysis of transonic buffet on a 3D swept wing using fast-response pressure-sensitive paint," *Exp. Fluids*, Vol. 59, No. 6, 2018, pp. 108.

[33]Trefethen, L. N., Trefethen, A. E., Reddy, S. C., and Driscoll, T. A., "Hydrodynamic Stability Without Eigenvalues," *Science*, Vol. 261, No. 5121, 1993, pp. 578–584.

[34]Crouch, J. D., Garbaruk, A., and Strelets, M., "Global Instability Analysis of Unswept- and Swept-Wing Transonic Buffet Onset," *2018 Fluid Dynamics Conference, AIAA AVIATION Forum*, 2018, AIAA 2018-3229.

[35]Theofilis, V., "Global Linear Instability," *Annu. Rev. Fluid Mech.*, Vol. 43, No. 1, 2011, pp. 319–352.

[36]Sipp, D. and Lebedev, A., "Global stability of base and mean flows: a general approach and its applications to cylinder and open cavity flows," *J. Fluid Mech.*, Vol. 593, 2007, pp. 333–358.